Journal of Materials Chemistry A

ROYAL SOCIETY OF CHEMISTRY

PAPER

View Article Online
View Journal | View Issue

Cite this: *J. Mater. Chem. A*, 2021, **9**, 22901

Enhanced hydrogen evolution efficiency achieved by atomically controlled platinum deposited on gold nanodendrites with high-index surfaces†

Ying-Huang Lai, *[a] Sin-Ren Li,‡[a] Swathi M. G,‡[a] Hsiao-Tzu Chang,‡[a] Yu-Bin Huang,[a] Yen-Ken Li,[a] Yu-Mei Chen,[a] Shivaraj B. Patil,[a] Shu-Yi Chang,[a] Po-Kai Chen,[a] Chia-Che Chang,[a] Yi-Chia Chen,[a] Chih-Wen Pao,[b] Jeng-Lung Chen, [b] Chuan-Yu Wei,[c] I.-Kuan Lin,[c] Hung-Lung Chou,[d] Chun-Jen Su,[b] U-Ser Jeng, [be] Tsung-Rong Kuo, [f] Cheng-Yen Wen [cgh] and Di-Yan Wang *[a]

There have been several studies on the catalytic activity of the hydrogen evolution reaction (HER) using ultralow loading of Pt catalysts or even Pt single atom catalysts. However, Pt single atom deposited on the surface of the carbon or metal oxide material has some drawbacks, such as high possibility of Pt desorption from the supported material in the electrolyte. Besides, from the reaction mechanism perspective, each Pt atom in this type of catalyst is too far to achieve high HER efficiency *via* the Tafel reaction pathway. In this work, gold nanodendrites (Au NDs) with high facet surface were chosen as the supported materials for studying the relation between the low loading amount of Pt atoms and the reaction mechanism of the HER activity. The atomic deposition of Pt atoms on the surface of Au NDs can be controlled effectively using a constant-current synthetic method. It was found that the HER electrocatalytic activity of ultralow Pt loading catalyst, with Pt atoms to total surface atoms of Au NDs (O-Pt on Au NDs) of 5.5%, could achieve high efficiency *via* the Tafel reaction pathway, showing a low overpotential of ~18 mV at a current density of 10 mA cm^{-2} and a small Tafel slope of ~31 mV dec^{-1}, which is close to that of commercial Pt/C with 20 wt% Pt. As confirmed by Inductively Coupled Plasma Mass Spectrometry(ICP-MS), the Pt loading amount of O-Pt on Au NDs was ~3.8 ± 0.2 μg cm^{-2} on a physical area of carbon fiber paper. The turnover frequency (TOF) of O-Pt on Au NDs was found to be 40.1 ± 2.5 H_2 per s at 50 mV. This work provides a feasible approach to control the atomic deposition of Pt on a specific substrate as an active catalyst for various catalytic applications.

Received 18th August 2021
Accepted 16th September 2021

DOI: 10.1039/d1ta07066e

rsc.li/materials-a

Introduction

Hydrogen has been considered as an encouraging chemical fuel that is a clean, sustainable, and feasible carrier candidate for green energy. The hydrogen produced from water electrocatalysis as an alternative to the cracking process of fossil fuels has exhibited the advantage of zero carbon emission. To date, noble metal catalysts, such as platinum (Pt) catalysts, are identified as the most effective water electrocatalysts, having the best kinetics for the hydrogen reduction reaction (HER) with a Tafel slope of 30 mV dec^{-1} and a low overpotential (0 V *vs.* RHE) in acidic media.[1–4] Recently, the development of low Pt content electrocatalysts is an efficient approach to reduce the amount of Pt while still maintaining its high activity.[5,6] Pt single-atom catalysts for HER were fabricated by

[a]*Department of Chemistry, Tunghai University, Taichung 40704, Taiwan. E-mail: yhlai@go.thu.edu.tw; diyanwang@thu.edu.tw*

[b]*National Synchrotron Radiation Research Center, Hsinchu 30076, Taiwan*

[c]*Department of Materials Science and Engineering, National Taiwan University, Taipei 10617, Taiwan*

[d]*Graduate Institute of Applied Science and Technology, National Taiwan University of Science and Technology, Taipei 106, Taiwan*

[e]*Chemical Engineering Department, National Tsing-Hua University, Hsinchu, 30013, Taiwan*

[f]*Graduate Institute of Nanomedicine and Medical Engineering, International PhD Program in Biomedical Engineering, College of Biomedical Engineering, Taipei Medical University, Taipei 11031, Taiwan*

[g]*Center of Atomic Initiative for New Materials, National Taiwan University, Taipei 10617, Taiwan*

[h]*International Graduate Program of Molecular Science and Technology, National Taiwan University, Taipei 10617, Taiwan*

† Electronic supplementary information (ESI) available: It contains additional XPS spectra, CV plot, UV spectra, Tafel for light illumination and SEM images, LSV plot, Tafel plot, and Raman spectra for Ag NDs and Cu NDs, and also the XRD spectra of pristine Au NDs and O-Pt on Au NDs. Tables list the recent HER performance and the TOF value for comparison. See DOI: 10.1039/d1ta07066e

‡ Sin-Ren Li, Swathi M. G and Hsiao-Tzu Chang contributed equally to this work.

decorating the surface of the supporting material with isolated Pt atoms.[7–10] Each Pt atom acts as active sites to adsorb the proton for HER with increased H_2 turnover frequency (TOF). For example, Pt atom-supported onion-like carbon catalyst (0.27 wt% of Pt loading) exhibited good HER performance with an overpotential of 38 mV (@10 mA cm^{-2}) and a TOF of 40.87 H_2 per s at 100 mV.[11] Also, different approaches to prepare single atom Pt-based catalysts have also been demonstrated and have exhibited good HER activity[12–14] However, single atom deposited on the surface of the supporting material tends to undergo aggregation to form clusters or dissolve in the solution during the long-term catalytic process, hampering the advantages of single atom toward HER.[7,15–17] Besides, Pt in Pt single-atom catalysts easily forms a chemical bond with oxygen atom, showing that it could have hindered the Pt atom from adsorbing the proton to form the Pt–H bond.[11,18–22] Besides, the reaction mechanism of single atom Pt-based catalysts for HER is almost impossible to be achieved using the Tafel reaction because Pt atom in this kind of a catalyst was far too separated to carry out the reaction of the two adsorbed atomic hydrogen on adjacent Pt atoms and then combine to form molecular hydrogen.[12,17] Therefore, it is still challenging to develop an active surface with the lowest Pt loading to achieve stable HER activity *via* the Tafel reaction pathway.

Owing to an abundance of terraces, steps, kinks, and vacancies covering the surface, metal nanostructures with a high surface index can be considered as highly active catalysts. They also possess higher surface energy, which enhances the adsorption of the reactant and improves the catalytic activity.[23–29] However, the active sites of the high index surface can also be occupied by contaminations such as those by salt ions or surfactants during the preparation process or electrochemical reaction, resulting in diminished catalytic performance. Therefore, the deposition of lower Pt atoms on the metal support with high index surface can be considered as a potential approach to achieve high HER activity.

Herein, we present the ingenious fabrication of minimum Pt atom-deposited Au nanodendrites (NDs) with high index surface by the electrochemical deposition method. Two steps of the electrochemical protocol (Fig. 1) were constructed, including step 1 involving the cyclic voltammetry (CV) scan in 0.5 M KOH and step 2 involving long-term amperometric (*i*–*t*) curve in 0.5 M H_2SO_4 electrolyte with a potentiostatic function. In step 1, the CV scan was carried out in the potential window from +0.4 V to −0.8 V in 0.5 M KOH at a rate of 10 mV s^{-1} with the as-prepared Au NDs, a carbon rod, and saturated calomel electrode as the working, counter, and reference electrodes, respectively. The CV scan in KOH was intended to effectively remove the contaminants such as sulphate and cysteine molecules from the surface of the as-prepared Au NDs to form pristine Au NDs with a clean high facet surface. It was followed by the deposition of Pt atoms on the Au NDs by applying a constant potential (−0.10 V *vs.* RHE, without *iR* compensation) over 5.5 h. According to detailed structural analysis including CV studies, X-ray photoemission spectra (XPS), and *in situ* X-ray absorption spectra (XAS), the deposition amount of Pt atoms on the surface is only 5.5% in comparison with Au atoms on the surface of the Au nanodendrites. As analyzed by inductively coupled plasma mass spectrometry (ICP-MS), the Pt loading amount on the Au NDs is only 3.8 ± 0.2 μg cm^{-2}. Interestingly, very few Pt atoms on Au NDs manifested superior catalytic activity toward HER by achieving a Tafel slope of ~31 mV per decade, which is very close to that of the commercial Pt/C electrode. The characterization and results are discussed in the subsequent sections.

Results and discussion

Fig. 2a shows the schematic representation of the electrochemical three-electrode system with Pt wire as the counter electrode, SCE as the reference electrode, and pristine Au NDs

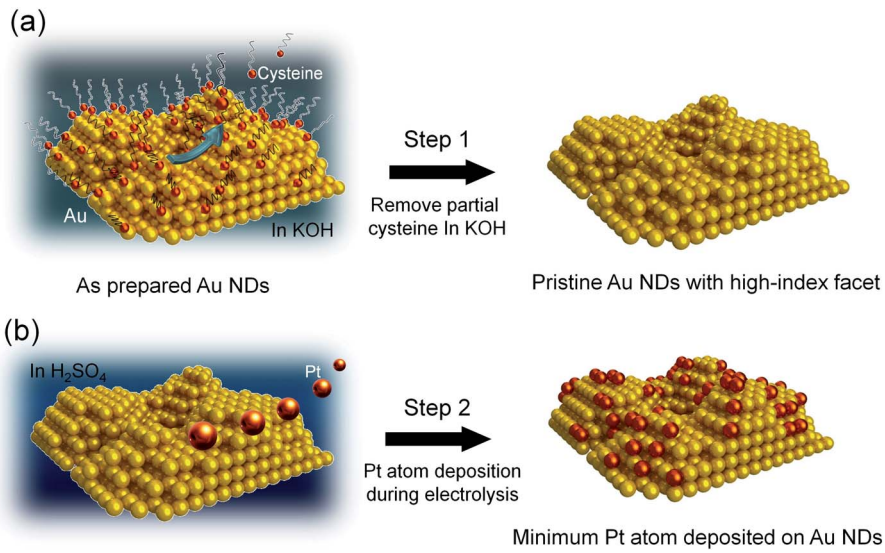

Fig. 1 Schematic representation of the proposed mechanism of (a) the formation of Au NDs with a clean high-index surface and (b) a controllable-minimum amount of Pt deposition on its surface in two steps.

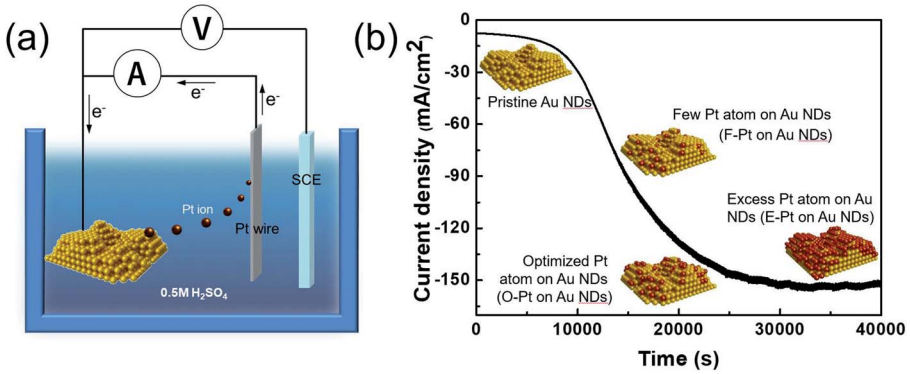

Fig. 2 (a) Schematic representation of the three-electrode system for the controllable fabrication of Pt atoms deposited on Au NDs. (b) Long term *i*–*t* curve of the Au NDs with an applied constant potential of −0.10 V (*vs.* RHE, without *IR* compensation) in 0.5 M H_2SO_4 solution was maintained and an in-site schematic illustration of the Au NDs with different deposition amounts of the Pt atoms over different time intervals has been included.

as the working electrode. The deposition amount of the Pt atoms on the surface of the Au NDs can be controlled by the chronoamperometric (*i*–*t*) method in 0.5 M H_2SO_4 by applying a voltage of −0.10 V. Fig. 2b shows the long-term *i*–*t* curve for Pt deposition on Au NDs. The current density was found to be improved with an increase in the reaction time, meaning that the HER activity is improved during this process. To ensure that the Pt ions are oxidized and dissolved slowly from the counter electrode into the acid electrolyte, ICP-MS measurements were carried out to detect the concentration of Pt ions in the electrolyte during the reaction. The concentration of Pt ions existing in the electrolyte was measured to be ∼100 ppb. Therefore, the improved effect of the current density can be ascribed to the gradual and slow deposition of the Pt atom on the surface of the Au NDs. The schematic illustration of the deposition amount of Pt atoms on the Au NDs over different time intervals is shown in Fig. 2b. At the beginning, when the current started to increase, few Pt atoms were loaded onto the Au NDs (F-Pt on Au NDs). After that, the current density was continually increased with time and reached saturation, meaning that the optimized amount of the Pt atoms deposited on the Au NDs was achieved (O-Pt on Au NDs). At the end of the reaction (40 000 s), excess of Pt atoms were loaded onto the Au NDs (E-Pt on Au NDs). Further characterization and reactions were carried out using these samples. After the completion of the electrochemical deposition method, the working electrode was carefully removed from the system and placed in another cell using carbon rod as the electrode containing 0.5 M H_2SO_4 solution for conducting further catalytic reactions.

Fig. 3a displays the scanning electron microscopy (SEM) image of representative O-Pt on Au NDs on the CFP. The results showed that there was a wide range of dendrite-like structures on the electrode surface. The structure consists of many micrometer-grade main stems and side branches as well as numerous small protrusions, high-curvature edges, and tips. This structural feature can create highly specific surface area and many high-aspect active sites. The transmission electron microscopy (TEM) image further illustrated the hyper-branched hierarchical structure of O-Pt on the Au NDs in Fig. 3b. Fig. 3c and d present the scanning transmission electron microscopy (STEM) images of O-Pt on the Au NDs. The result showed that the single crystal structure of the branch of O-Pt on the Au NDs was found to have a highly ordered continuous fringe pattern, which exposed the {111} facet. Further, high-index facets (pointed by the red spot) exposed on the surface of the branch was also revealed. The Fast Fourier Transforms (FFT) image (Fig. 3e) indicated that O-Pt on the Au NDs also revealed several index facets including {111}, {200}, {220}, and high-index {311} facets. The overall results confirmed the formation of highly branched O-Pt on the Au NDs with highly oriented homogeneous phases and edges.

To investigate the loading amount of the Pt atoms on the Au NDs, the mapping of time-of-flight secondary ion mass spectrometry (TOF-SIMS) and ICP-MS analysis were carried out, as shown in Fig. 4 and Table S1†, respectively. For the as-prepared Au NDs, there are obvious and uniform signals of Au and S found in the as-prepared Au NDs (Fig. 4a), meaning that there is containment of cysteine on the surface of the as-prepared Au NDs before KOH treatment. After being treated with KOH, there was nearly no S signal observed in the pristine Au NDs (Fig. 4b). Fig. 4c shows the mapping of the Au and Pt elements of O-Pt on the Au NDs. Few signals of Pt were also observed along with Au NDs, confirming the loading of few Pt atoms over the Au NDs. The corresponding schematic diagrams are provided as the insets in Fig. 4. Furthermore, ICP-MS analysis indicated that the Pt loading amount of F-Pt on Au NDs, O-Pt on Au NDs, and E-Pt on Au NDs is 0.061%, 0.19%, and 0.51%, respectively.

X-ray absorption fine structure (XAFS) spectroscopy has been widely applied in studies related to catalytic materials.[30–33] X-ray absorption near edge structure (XANES) reveals the orbital hybridization between the absorbing and the coordinate atoms, while the extended X-ray absorption fine structure (EXAFS) gives the local structure parameters such as coordination number, bond length, and Debye–Weller factor in materials. Although the atomic distribution of bimetallic nanoparticles can be

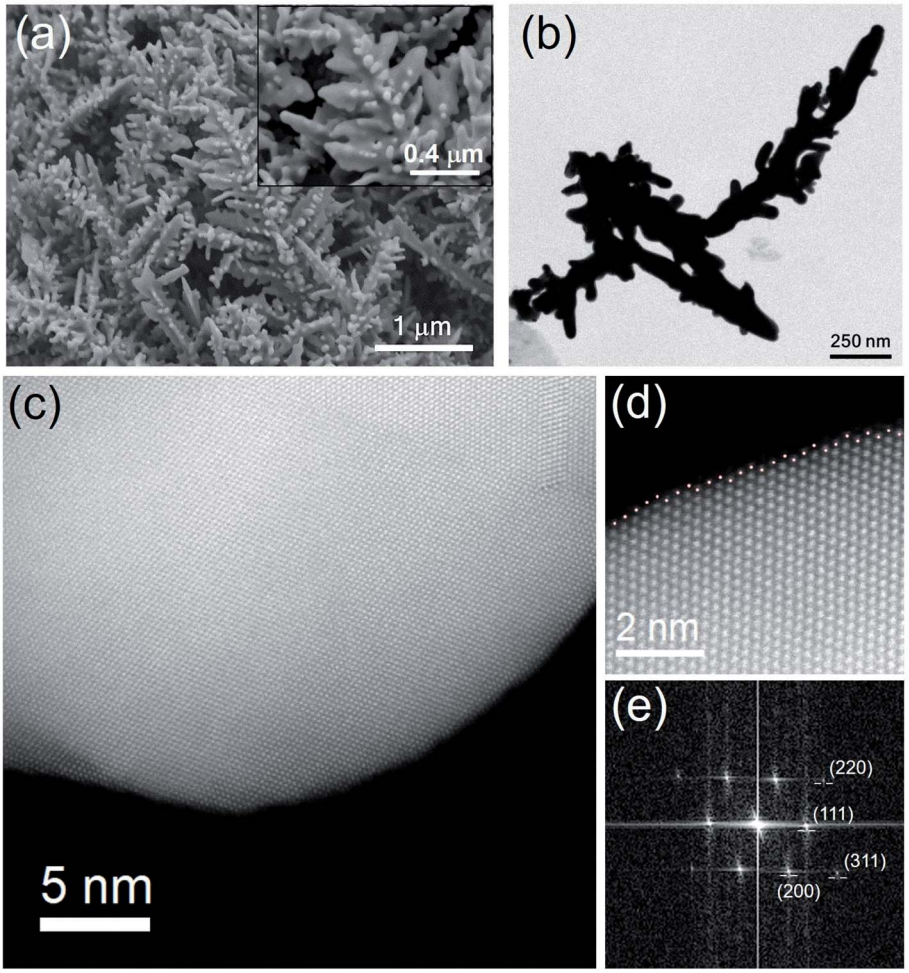

Fig. 3 (a) SEM image and (b) TEM image of O-Pt on the Au NDs structures grown on the CFP electrode. (c) STEM image of O-Pt on Au NDs and (d) the higher magnification of the STEM image recorded from the branch of O-Pt on the Au NDs shown in (c). (e) FT patterns of O-Pt on the Au NDs surface indicates that the branch was enclosed by (111), (200), (220), and high index (311) facets.

evaluated through the total coordination number from EXAFS analysis, it is not easy to resolve the core–shell structure in the case with high concentration ratio of different elements in the structure. In addition, the similar scattering amplitude of Pt and Au atoms leads to poor species resolution of the first coordination atoms using the EXAFS method. However, the elemental resolution of EXAFS spectroscopy still provides a revelation of the heteroatomic interaction on Pt and Au atoms. Fig. 5 displays the normalized XANES spectra at Au and Pt L_3-edge of pristine Au NDs, F-Pt on Au NDs, O-Pt on Au NDs, E-Pt on Au NDs, and the reference standards of Pt and Au. The high overlapping of the spectra at the Au L_3-edge XANES spectra of the Au NDs samples and the standard Au foil indicate that the Au atom of each sample is in the metallic state (Fig. 5a). In the Pt L_3-edge XANES spectra (Fig. 5b), the increased white-line (WL) intensity and the energy shift of the WL peak position is associated with the interaction between the Pt and Au atoms.[9,34] This phenomenon is not obvious as the Au L_3-edge XANES spectra is due to the much larger concentrations of the Au atoms in comparison with that of the Pt atoms. The Fourier-transform (FT) EXAFS spectra of the pristine Au NDs, F-Pt on Au NDs, O-Pt on Au NDs, and E-Pt samples on the Au NDs at the Au L_3-edge (Fig. 5c) indicate that the Au atom of each sample is in the metallic state, which is consistent with the results of the Au L_3-edge XANES spectra. The major different feature at 2.2 Å of the FT-EXAFS spectra at the Pt L_3-edge (Fig. 5d) corresponds to the nearest-neighbor (Pt–Au and Pt–Pt bond) contributions. The intensity of the FT-EXAFS spectra for the Pt–Au and Pt–Pt bonds is proportional to the diameter of the structural size; therefore, it can be utilized to evaluate the distribution range of Pt atoms on the Au NDs.[11,12,18,35,36] The increased intensity of the peak (~2.2 Å) at the Pt L_3-edge FT-EXAFS spectra indicates the increase in the distribution range of the Pt atom on the NDs samples with the electrochemical deposition time. The overall results represent that the distribution size of the Pt atoms deposited on the surface of O-Pt on the Au NDs is smaller than 2 nm.

To analyze the surface composition and oxidation state of pristine Au NDs, F-Pt on Au NDs, O-Pt on Au NDs, and E-Pt on Au NDs, the XPS spectra using an incident X-ray source of 250 eV were used to observe about 0.7 nm-depth according to the estimation of the inelastic mean free path of the

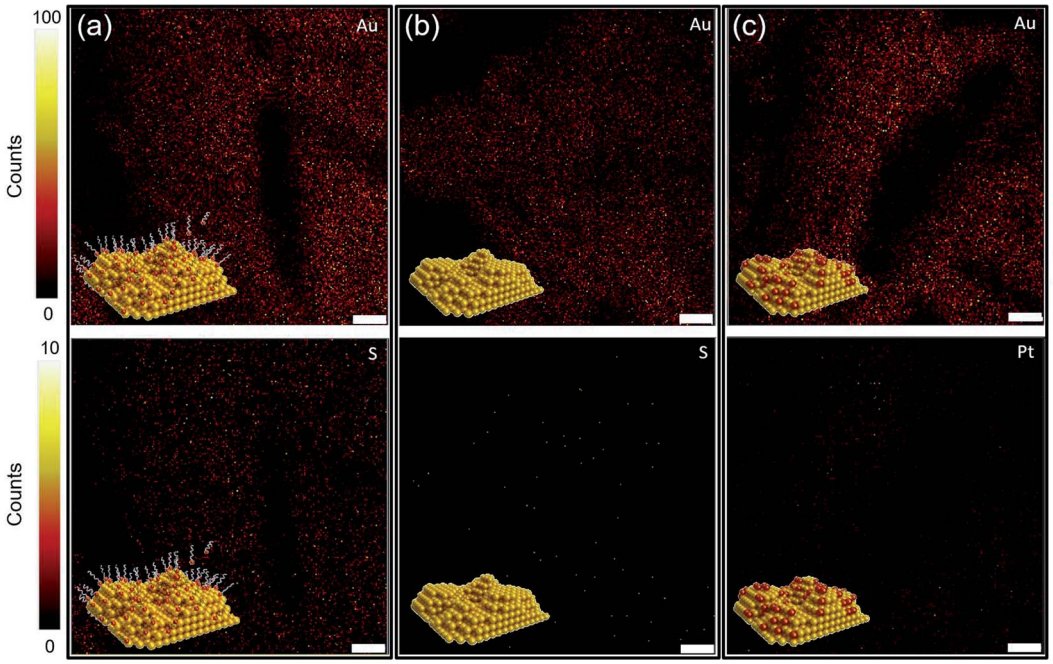

Fig. 4 TOF-SIMS mapping images of (a) as prepared Au NDs, (b) pristine Au NDs and (c) O-Pt on Au NDs. The signals were collected from different ions, including Au^+, cysteine cation and Pt^+ and emitted from an area of 10 × 10 μm^2.

electrons.[37] In Fig. 6a, the XPS spectrum analysis of Au 4f shows that the binding energy of Au $4f_{7/2}$ in each sample is the same as that of the standard sample, which is located at 84.0 eV, meaning that the Au element in all the samples remained in the metallic state. Fig. 6b shows the XPS spectra of Pt $4f_{7/2}$ of F-Pt on Au NDs, O-Pt on Au NDs, and E-Pt on Au NDs. A less intense signal of Pt was observed in F-Pt on the Au NDs, indicating that the deposition amount of Pt on the surface of the Au NDs is much less than 1%. There is an obvious Pt signal found for the other two samples. There are doublet peaks found at 70.9 eV and 74.8 eV, which can be deconvoluted into two peaks. The deconvoluted peaks at 70.9 eV and 74.8 eV, 71.6 eV and 74.5 eV can be ascribed to the surface Pt atoms deposited on the low index facet surface and partially oxidized Pt deposited on the high index faceted surface, respectively.[34] There is no obvious metallic state of Pt observed in these Pt deposited on the Au NDs samples. Although the signals of Au 5p and Pt $4f_{5/2}$ overlap each other, the low intensity of Au 5p can be ignored, meaning that the signal of Pt $4f_{7/2}$ is not affected. To investigate the ratio of Pt and Au on the surface of O-Pt on Au NDs and E-Pt on Au NDs, the integrated areas of the deconvoluted peaks in the Pt 4f and Au 4f XPS spectra were quantified and the results are presented in Table 1. The area corresponding to Pt on the surface of O-Pt on Au NDs and E-Pt on Au NDs is 5.5% and 20.3%, respectively. The overall results indicated that the O-Pt on Au NDs has only 5.5% of Pt atoms deposited on the surface of the Au NDs and its Pt atoms have two kinds of chemical environments, including the reduced state of the surface metal (Pt $4f_{7/2}$ = 70.8 eV) and the partially oxidized state (Pt $4f_{7/2}$ = 71.7 eV).

In order to test the electrochemical catalytic performance of the catalysts in HER, linear sweep voltammetry (LSV) of the as-prepared Au NDs with cysteine contaminant, pristine Au NDs, F-Pt on Au NDs, O-Pt on Au NDs, E-Pt on Au NDs, and commercial Pt/C with 20 wt% Pt was carried out in 0.5 M H_2SO_4 solution at a sweep rate of 5 mV s^{-1} using a three-electrode system including SCE as the reference electrode and carbon rod as the counter electrode. Additional *iR* compensation was applied during the LSV measurement to remove the external resistance of the electrode/electrolyte system. In Fig. 7a, the overpotential of the as-prepared Au NDs for HER is 240 mV at a current density of 10 mA cm^{-2}. This result can be attributed to the structural characteristics of dendritic gold. After removing cysteine, the overpotential of pristine Au NDs for HER is reduced to 175 mV at a current density of 10 mA cm^{-2}. This could be attributed to the exposure of a clean high index surface of the Au NDs by the removal of cysteine and the creation of numerous active sites for HER. Moreover, when Pt atom was gradually deposited onto the Au NDs, the overpotential of F-Pt on the Au NDs decreased to ~70 mV at a current density of 10 mA cm^{-2}. In particular, the lowest overpotential of O-Pt on Au NDs was achieved to ~18 mV at a current density of 10 mA cm^{-2}, which is close to that of commercial Pt/C and E-Pt on Au NDs. The current density of 100 mA cm^{-2} of O-Pt on Au NDs for HER can be achieved dramatically by slightly increasing the potential to −0.05 V. The Tafel slope is a useful metric to assess the performance of the catalysts and is a valuable indicator of the mechanistic reaction processes of HER. Fig. 7b shows the Tafel slope of the Au NDs when it was treated under different conditions. The Tafel slope of pristine Au NDs treated with KOH was calculated to be ~71 mV dec^{-1}, which is closer to that of the as-prepared Au NDs (~70 mV dec^{-1}). Interestingly, after Pt deposition on the Au NDs, the Tafel slope of F-Pt on the Au NDs decreased to ~51 mV dec^{-1} and that of O-Pt on Au NDs was

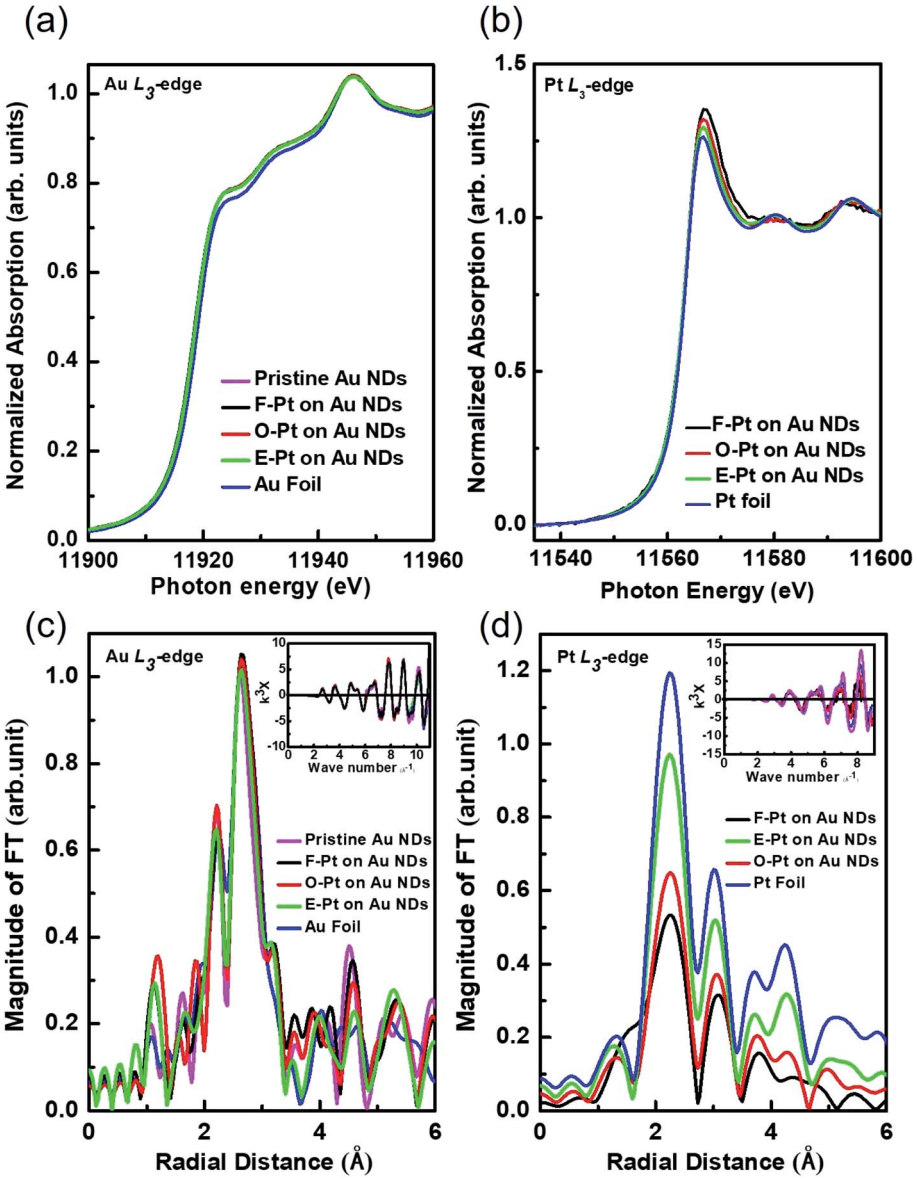

Fig. 5 (a) Normalized XANES spectra near the Au L_3-edge of pristine Au NDs, F-Pt on Au NDs, O-Pt on Au NDs, E-Pt on Au NDs, and Au foil. (b) Normalized XANES spectra near the Pt L_3-edge of F-Pt on Au NDs, O-Pt on Au NDs, E-Pt on Au NDs, and Pt foil. (c) FT-EXAFS spectra at the Au L_3-edge of Au NDs, F-Pt on Au NDs, O-Pt on Au NDs, E-Pt on Au NDs, and Au foil. (d) FT-EXAFS spectra at the Pt L_3-edge of F-Pt on Au NDs, O-Pt on Au NDs, E-Pt on Au NDs, and Pt foil. (c) and (d) Inset shows the Au L_3-edge and Pt L_3-edge EXAFS oscillation of each sample, respectively.

achieved to be ~31 mV dec^{-1}, similar to that of the Pt/C catalyst (31 mV dec^{-1}) and E-Pt on Au ND (31 mV dec^{-1}). The slope of the Tafel plot also reveals that the reaction mechanism of O-Pt on the Au NDs for HER refers to the Tafel reaction as the rate-determining step for HER. To quantify the catalytic efficiency of the active Pt site on the O-Pt on Au NDs, the turnover frequency (TOF) was also calculated and is presented as shown in Fig. 7c. We found that the TOF can be achieved as high as 40.1 ± 2.5 H_2 per s at an η of 50 mV for O-Pt on Au NDs, which is better than that of the pristine Au NDs and commercial Pt/C. These results imply that the excellent catalytic activity of O-Pt on Au NDs can be ascribed to the complete utilization of Pt atoms on the surface of the Au NDs. Furthermore, the long-term stability of O-Pt on Au NDs was investigated by the amperometric current density–time response over 85 h by applying a constant potential of −0.06 V, as shown in Fig. 7d. A high current density was maintained at 100 mA cm^{-2} over 85 h, signifying the excellent stability and activity of O-Pt on Au NDs for HER.

As we know, the effect of surface plasmon resonance (SPR) could promote the performance of the hydrogen evolution process. We further discuss the effect of SPR to improve the HER performance of O-Pt on the Au NDs. At room temperature, the three-electrode HER reaction system in 0.5 M H_2SO_4 solution used AM1.5G light source to provide 100 mW cm^{-2} energy. The applied potential was fixed at −16 mV (*vs.* RHE,

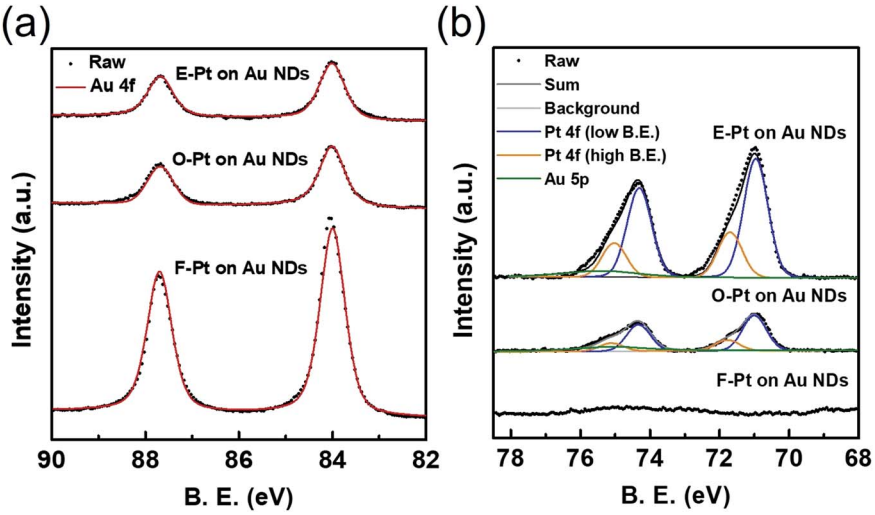

Fig. 6 (a) Au 4f and (b) Pt 4f XPS spectra of F-Pt on Au NDs, O-Pt on Au NDs, and E-Pt on Au NDs. The incident X-ray photon energy is 250 eV.

Table 1 Binding energy (eV) and atomic ratios of Pt and Au obtained from the XPS spectra of O-Pt on Au NDs and E-Pt on Au NDs

	Peak	Peak (eV)	Area/cross section	Pt ratio (to Au 4f)	
O-Pt on Au NDs	Pt $4f_{7/2(\text{low B.E})}$	70.92	457.0	0.042	0.054
	Pt $4f_{7/2(\text{high B.E})}$	71.68	140.8	0.013	
	Au $4f_{7/2}$	84.00	11 074		
E-Pt on Au NDs	Pt $4f_{7/2(\text{low B.E})}$	70.96	1616	0.148	0.203
	Pt $4f_{7/2(\text{high B.E})}$	71.7	596.1	0.055	
	Au $4f_{7/2}$	84.00	10 929		

with additional *IR* compensation). In Fig. 8, we observed that during the period when the light was switched on for 60 s and the light was switched off for 240 s, the photocurrent increased immediately with light-on and decreased suddenly with light-off. The current density changes can be divided into four stages, as shown in the inset. In the first stage, after illuminating on the working electrode, the current density rises immediately from 10 to 10.7 mA cm^{-2} in two seconds, which could be originated from the photoelectric enhancement. At this stage, a plasma resonance effect occurs on the surface of O-Pt on Au NDs by the incident photons to generate a large number of surface electron oscillations at high frequencies at the active position of the reaction, resulting in improved electron-transfer efficiency of the reaction. In the second stage, the current density gradually increased from 10.7 to 11.4 mA cm^{-2} after light incidence from 2 to 60 s, caused by the high-frequency movement of the surface plasma at this time and the catalyst surface temperature increases, which called the photothermal effect.[38] In the third stage, when the light source is secluded, an instantaneous drop in the equivalent HER rate can be observed. The shading current density of the light source decreased from 11.4 to 10.7 mA cm^{-2} within 2 s (60–62 s). In the last stage, the current density decreases exponentially 2 s after the light source was secluded. It took about 120 s (62–182 s) to decrease from 10.7 to 10 mA cm^{-2}. Therefore, it took a long time for the surface temperature to return to the surface temperature before the illumination. The Tafel slope was verified to be the same before and after illuminated by light (Fig. S5†). The results represented that through the assistance of SPR to accelerate the HER activity, the rate-determining step of the reaction mechanism of O-Pt on the Au NDs still maintained the Tafel process.

Discussion

In order to realize the relationship between the stepwise deposition of Pt atoms on the Au NDs and the corresponding HER activity in the constant current synthesis method, *in situ* XAS measurements and the corresponding electrochemical properties were performed for Pt deposition on the Au NDs at different deposition times, as shown in Fig. 9. The results show that the white-line intensity and peak position in the Pt L_3-edge XANES spectra change significantly with the increase in the deposition time. The highest white-line intensity in the Pt L_3-edge XANES spectra was found at the start of the deposition time of 1.5 hours. As the deposition time increases, the white-line intensity gradually decreases and the peak slowly moves to the left, gradually approaching the reference Pt foil. This trend suggests that at the beginning of the deposition time, a minority of Pt atoms are deposited alone on the surface of the Au NDs separately, forming strong Pt–Au bonds (similar to the PtAu alloy),[39] resulting in much higher 5d electron vacancies in higher white-line intensities. The deposition size of the Pt atoms on the surface of the Au NDs increases with increasing deposition time, resulting in fewer vacancies in the 5d orbitals of Pt.

The experimental results presented in this work indicate that the excellent catalytic activity and stability of O-Pt on the Au NDs (deposition time of Pt ~11 h) for HER can be ascribed to the following important aspects. First, the constant low concentration of the Pt ions (0.1 ppm) in the electrodeposition system results in the Pt atoms being allowed to be deposited slowly and

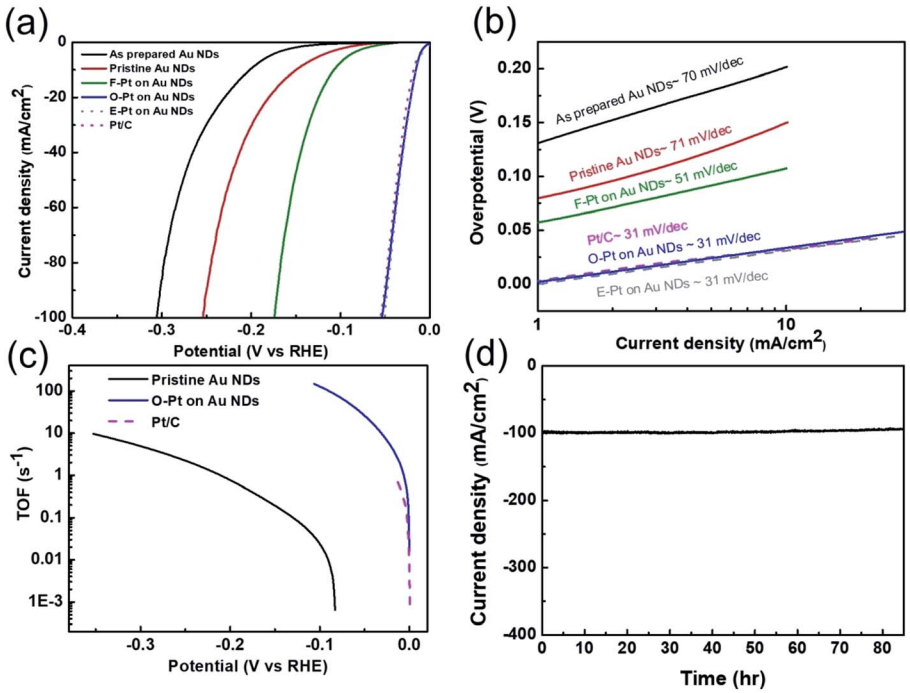

Fig. 7 (a) Polarization curves at a scan rate of 5 mV s^{-1} obtained with a series of Pt on Au NDs catalysts and (b) the corresponding Tafel plots recorded from the as-prepared Au NDs, pristine Au NDs, F-Pt on Au NDs, O-Pt on Au NDs, E-Pt on Au NDs, and Pt/C loading of 1 mg cm^{-2} (c) TOF curve of pristine Au NDs, O-Pt on Au NDs, and Pt/C. (d) Current *versus* time during long term use (85 h) with a constant potential (−0.06 V) electrolysis of O-Pt on Au NDs.

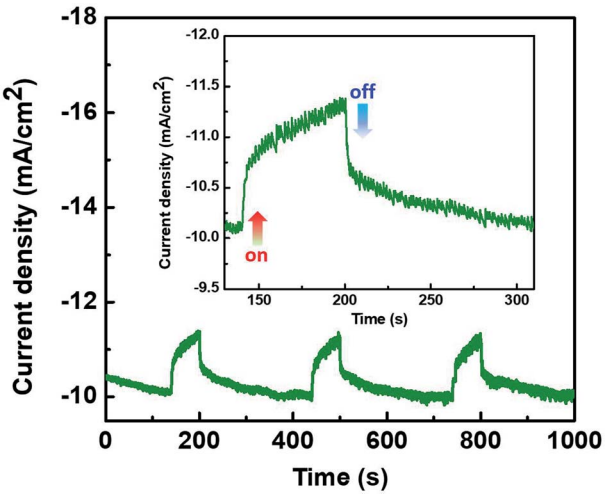

Fig. 8 Chronoamperograms during the on/off light switching test for O-Pt on Au NDs under AM1.5G light (with a water filter) and in the dark in a 0.50 M H_2SO_4 solution at −16 mV, which was maintained for 1000 s. Illumination power density on the working electrode was 100 mW cm^{-2}. Inset window is the first-cycle chronoamperogram during the on/off light switching test.

preferentially on the surface of the Au NDs with terraces, steps, kinks, and vacancies of high surface energy.[26–28,40] Thus, for O-Pt on Au NDs, only 5.5% of Pt atoms deposited on the Au ND surface (with a Pt loading of only 0.38 ± 0.2 μg cm^{-2} based on the physical area of CFP) can exhibit great HER activity, achieving Tafel reactions and TOF ~40.1 ± 2.5 H_2 per s at 50 mV. Table S2† shows the Pt content *versus* the TOF values for the Pt catalysts on different substrates at certain overpotentials, including the recently reported atomic metal species supported on carbon supports.[11,41,42] Our catalysts show strong competitiveness in hydrogen evolution reactions compared to other materials, such as Pt single atom on graphdiyne,[14] low Pt on graphitic tube,[13] Pt on carbon support,[11] and Pt-decorated graphene nanospheres.[43] Second, Au NDs with inner property play an important role in stabilizing the Pt atoms deposited on high surface energy sites for long-term reactions. To investigate the role of Au NDs as substrates for Pt deposition, Ag NDs and Cu NDs were obtained as substrates for Pt atom deposition by the same method as that for Au NDs. The HER activity of the O-Pt on Ag NDs and O-Pt on Cu NDs catalysts was measured in a three-electrode system with 0.5 M H_2SO_4 (see ESI, Fig. S2†). The results showed that the HER activity of O-Pt on Ag NDs and O-Pt on Cu NDs was enhanced with an overpotential of 0.129 V and 0.137 V at a current density of 20 mA cm^{-2} and a small Tafel slope of 61 mV dec^{-1} and 62 mV dec^{-1}, respectively. Although the catalytic performance of Ag NDs and Cu NDs was improved after the successful deposition of Pt atoms, the reaction mechanism of HER only reached the Heyrovsky–Tafel process. This may be due to the fact that the surfaces of Cu NDs and Ag NDs are more susceptible to oxidation, causing the high energy surfaces to become more unstable and unable to deposit Pt atoms successfully. The overall results show that unexpected HER catalytic activity can be achieved with small Pt deposition rates on the appropriate substrates.

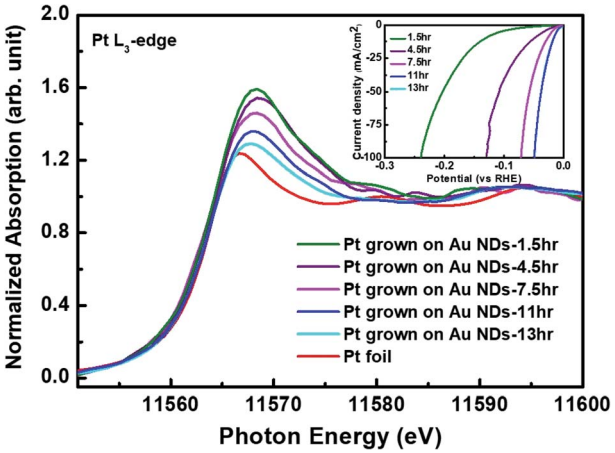

Fig. 9 Series of time-resolved Pt L_3-edge XANES of Pt atoms deposited on the surface of Au NDs during the deposition time. The inset is the corresponding polarization curves at a scan rate of 5 mV s^{-1} obtained with a series of Pt atoms grown on Au NDs.

Conclusion

In summary, Au NDs with clean high index surfaces have been successfully fabricated as active substrates for the selective deposition of Pt atoms. Furthermore, through a constant-current deposition method in acidic condition, we found that only 5.5% of Pt atoms deposited on the surfaces of Au NDs (O-Pt on Au NDs) can obtain excellent catalytic performance, exhibiting an overpotential of ~18 mV at a current density of 10 mA cm^{-2}, which is close to that of commercial Pt/C. It achieved the Tafel reaction showing a very small Tafel slope of ~31 mV dec^{-1}, which would be the fastest rate-determining step for HER. The turnover frequency (TOF) of O-Pt on the Au NDs was estimated to be 40.1 ± 2.5 H_2 per s at 50 mV. It was also found that light could slightly improve the HER performance of O-Pt on Au NDs *via* the surface plasma resonance effect. This study demonstrates the optimization technology for minimum Pt deposition on the surface of Au NDs (O-Pt on Au NDs) by creating a maximum catalytic active center on the surface to achieve superior HER performance.

Experimental section

Materials

Auric chloride ($HAuCl_4 \cdot 3H_2O$; ACS 99.9%) from Alfa Aesar, L-cysteine ($C_3H_7NO_2S$; Acros, >99%), copper(II) sulfate pentahydrate ($CuSO_4 \cdot 5H_2O$; ACS 99.0–100.5%), potassium hydroxide (KOH; ACS 85%), and sulfuric acid (H_2SO_4; 95–97%) were procured from Sigma Aldrich, and silver sulfate (Ag_2SO_4; ACS 99%) was procured from Scharlau. All the chemicals were used without further purification. Carbon fiber paper (CFP) was procured from CeTech Co., Ltd. and it was used as a substrate for deposition. Deionized water (DI H_2O) was used throughout the experiments.

The fabrication of Au NDs on CFP

The Au NDs grown on carbon fiber paper (CFP) were modified according to our previous report.[44] The electrodeposition of the Au NDs on CFP (1 × 2 cm^2 area but during the reaction, only 1 × 1 cm^2 was immersed into the electrolyte) was performed in an aqueous solution of 1.0 mM $HAuCl_4$ and 0.5 M H_2SO_4 in the presence of 0.1 mM cysteine with a conventional three-electrode system using square-wave potential pulse function. A saturated calomel electrode (SCE) and carbon rod were applied as the reference and counter electrodes, respectively. The function of square-wave potential pulses was applied on the CFP electrode at a frequency of 5 s^{-1} for 3000 s. The low and high potentials of the square-wave pulse were set at −0.8 and + 0.2 V (*vs.* SCE), respectively. Finally, the as-prepared Au NDs were obtained.

The surface cleaning protocol of Au NDs

The cysteine removal process was followed by a single step of electrochemical reaction to obtain Au NDs with a clean high index surface. In the first step, the as-prepared Au NDs with fully adsorbed cysteine were operated by the CV scan in a potential range between −0.4 V and −1.3 V (*vs.* SCE) in 0.5 M KOH solution. Then, the pristine Au NDs with a clean high index surface were obtained.

The atomically-controlled Pt deposition process on the surface of Au NDs

To control the deposition amount of the Pt atoms on the surface of the Au NDs, long term amperometric *i–t* curve was obtained. Pristine Au NDs with a clean high index surface were used as the working electrode with 0.5 M H_2SO_4 solution as the electrolyte in the three-electrode system by applying a constant voltage of −0.15 V. Therefore, the different deposition amounts of Pt atoms on Au NDs were obtained on increasing the reaction time.

Material characterization

A conventional three-electrode system in an electrochemical workstation (CHI 614B) was used for electrodeposition, where SCE served as the reference electrode and platinum wire as the counter electrode. The photoelectrochemical properties were examined in a three-electrode quartz cell to facilitate the illumination of the photoelectrode surface. The illumination source was a 300 W Xe arc lamp (Newport, 66901) directed at the quartz electrochemical cell (100 mW cm^{-2}) with an AM1.5G filter (Newport 81094). An IR water filter (Newport, 6123NS) was used to prevent the heating of the solution by infrared light. Thermal field emission scanning electron microscopy (FE-SEM) images were recorded on a JEOL JSM-6800F microscope operated at an accelerating voltage of 3.0 kV. The UV-vis absorption spectra of the samples were obtained using a Jasco V-770 spectrophotometer equipped with a spherical integrator ILN-925. The atomic ratio of the Pt and Au atoms was measured by the ICP-MS instrument (Thermo X Series II). The elemental mapping images of the materials were recorded by TOF-SIMS (ULVAC-PHI TRIFT IV). The powder XRD patterns were recorded on the BL23A SWAXS end station of the National Synchrotron Radiation Research Center, Taiwan, with an X-ray wavelength (λ) of 1.240 Å (10 keV).[45] The powder XRD data was recorded on an image plate, and the diffraction angle, 2θ, was

calibrated using diffractions from powder mixtures of silicon and silver behenate. The XPS spectra were recorded at the photoelectron spectroscopy (PES) end station of the NSRRC beamline 24A1. The onset of photoemission from a gold foil attached to the sample holder was used to calibrate the Fermi level as the zero-binding energy. The Au and Pt XPS spectra of the Pt/Au-Ds were recorded using an incident beam of X-ray energy at 250 eV. The Pt and Au L_3-edge X-ray absorption fine structure (XAFS) spectra of the F-Pt/Au, O-Pt/Au, and E-Pt Au nanodendrites (NDs) were performed at TPS-44A beamline of the National Synchrotron Radiation Research Center (NSRRC). The Au L_3-edge XAFS spectra were collected in the transmission mode, where the Pt L_3-edge XAFS spectra were obtained in the fluorescence mode using a 7-element detector. The corresponding reference foils were measured simultaneously to calibrate the energy of the incident X-ray photons. The data were analyzed following the standard procedure using the Demeters software package.[7]

Electrochemical measurements

The standard three-electrode system was used for the HER activity and durability measurements. Herein, the materials were used as the working electrode (on the CFP substrate of 1×1 cm^2 dimensions), whereas SCE was used as the reference electrode and carbon rod as the counter electrode. The linear sweep voltammogram tests were performed at a scan rate of 10 mV s^{-1} (with full *IR* compensation) in 0.5 M H_2SO_4 as electrolyte. All the potentials changed to RHE using the equation $E_{RHE} = E_{SCE} + 0.245\ V + 0.059 \times pH$.

The Tafel slope was calculated by fitting to the Tafel equation $\eta = b \log j + c$, where b is the Tafel slope, j is the current density, and c is the intercept relative to j_0. The exchange current density (j_0) value is calculated by the formula $j_0 = e^{(-2.303c/b)}$.

TOF calculation

First, the number of Pt atoms was determined from the electrochemically active surface area (ECSA), which was estimated from the desorption peak of Pt–H at 0.0 V, and the reduction peak of gold at 1.12 V was 4.7 cm^2 (Pt) and 76.3 cm^2 (Au). The Pt/Au ratio obtained by calculating the ECSA is about 6.1%, which is close to the value calculated by XPS analysis. Surface active Pt atoms per square meter area (supposed Pt atoms fully cover the surface with a radius ~139 pm) is

$$\frac{1}{\pi\left(1.39 \times 10^{-10}\ m\right)^2} = 1.647 \times 10^{19}\ \text{Pt atoms per } m^2$$
$$= 1.647 \times 10^{15}\ \text{Pt atoms per } cm^2$$

The number of Pt atoms on the active surface area of 4.7 ± 0.3 cm^2 is

$$1.647 \times 10^{15}\ \text{Pt atoms per } cm^2 \times 4.7\ cm^2 = 7.74 \times 10^{15}\ \text{Pt atoms}$$

Second, the total number of hydrogen turnover was calculated to be 3.12×10^{15} H_2 per s per mA.[11,13] The TOF per Pt site in the O-Pt on Au NDs catalyst for the HER is calculated by the equation

$$\text{TOF} = \frac{\text{Total number of hydrogen turnover/physical area}}{\text{Number of active sites/active area}}$$

The TOF at the current density of ~100 mA cm^{-2} of O-Pt on Au NDs (an overpotential of 0.05 V *versus* RHE electrode) is

$$\frac{3.12 \times 10^{15}\ H_2}{1\ s \times mA} \times 100\ mA \times \frac{1}{7.74 \times 10^{15}\ \text{Pt atoms}}$$
$$= 40.1 \pm 2.5\ H_2 \text{ per s per Pt atom}$$

Author contributions

Y. Lai and D. Wang conceived the project and designed the experiments. S. Li, S. MG, H. Chang, Y. Huang, Y. Li, Y. Chen, S. Patil, S. Chang, P. Chen, C. Chang and Y. Chen performed material preparation, structural characterization and electrochemical measurements. Y. Chen and Y. Chen helped perform the X-ray photoemission measurement and analyzed the data. C. Pao and J. Chen helped perform XAS measurement in the NSRRC. H. C. Wei, I-Lin and C. Wen helped performed STEM analysis. C. Su and U. Jeng helped perform XRD in the NSRRC. T. Kuo helped perform ICP-MS and TOF-SIMS analysis. Chou helped to perform DFT simulation. Y. Lai, S. MG and D. Wang co-wrote the paper. All authors discussed the results and commented on the manuscript.

Conflicts of interest

The authors declare no conflict of interest.

Acknowledgements

This work has been financially supported by the Ministry of Science and Technology of Taiwan (MOST 106-2113-M-029-006-MY2, MOST 106-2632-M-029-001, MOST 107-2622-M-029-001-CC2 and MOST 109-2639-E-011-001-ASP) and Tunghai University. We thank Dr U-Ser Jeng for assistance at beamline BL23A at Taiwan Light Source (TLS) and Dr Hwo-Shuenn Sheu, Dr Yu-Chun Chuang for assistance at beamline 09A at the Taiwan Photon Source (TPS).

References

1 H. Yin, S. Zhao, K. Zhao, A. Muqsit, H. Tang, L. Chang, H. Zhao, Y. Gao and Z. Tang, Ultrathin platinum nanowires grown on single-layered nickel hydroxide with high hydrogen evolution activity, *Nat. Commun.*, 2015, **6**(1), 1.

2 R. Subbaraman, D. Tripkovic, D. Strmcnik, K.-C. Chang, M. Uchimura, A. P. Paulikas, V. Stamenkovic and N. M. Markovic, Enhancing hydrogen evolution activity in water splitting by tailoring Li+-Ni (OH) 2-Pt interfaces, *Science*, 2011, **334**(6060), 1256.

3 D. V. Esposito, S. T. Hunt, A. L. Stottlemyer, K. D. Dobson, B. E. McCandless, R. W. Birkmire and J. G. Chen, Low-cost hydrogen-evolution catalysts based on monolayer platinum on tungsten monocarbide substrates, *Angew. Chem., Int. Ed.*, 2010, **49**(51), 9859.
4 F. Gao, Y. Zhang, Z. Wu, H. You and Y. Du, Universal strategies to multi-dimensional noble-metal-based catalysts for electrocatalysis, *Coord. Chem. Rev.*, 2021, **436**, 213825.
5 Z. Li, R. Ge, J. Su and L. Chen, Recent Progress in Low Pt Content Electrocatalysts for Hydrogen Evolution Reaction, *Adv. Mater. Interfaces*, 2020, 2000396.
6 F. Gao, Y. Zhang, F. Ren, Y. Shiraishi and Y. Du, Universal Surfactant-Free Strategy for Self-Standing 3D Tremella-Like Pd–M (M= Ag, Pb, and Au) Nanosheets for Superior Alcohols Electrocatalysis, *Adv. Funct. Mater.*, 2020, **30**(16), 2000255.
7 L. Zhang, L. Han, H. Liu, X. Liu and J. Luo, Potential-cycling synthesis of single platinum atoms for efficient hydrogen evolution in neutral media, *Angew. Chem., Int. Ed.*, 2017, **56**(44), 13694.
8 Z.-J. Chen, G.-X. Cao, L.-Y. Gan, H. Dai, N. Xu, M.-J. Zang, H.-B. Dai, H. Wu and P. Wang, Highly dispersed platinum on honeycomb-like NiO@ Ni film as a synergistic electrocatalyst for the hydrogen evolution reaction, *ACS Catal.*, 2018, **8**(9), 8866.
9 K. Tang, X. Wang, Q. Li and C. Yan, High Edge Selectivity of *In Situ* Electrochemical Pt Deposition on Edge-Rich Layered WS2 Nanosheets, *Adv. Mater.*, 2018, **30**(7), 1704779.
10 J. Chen, Y. Yang, J. Su, P. Jiang, G. Xia and Q. Chen, Enhanced activity for hydrogen evolution reaction over CoFe catalysts by alloying with small amount of Pt, *ACS Appl. Mater. Interfaces*, 2017, **9**(4), 3596.
11 D. Liu, X. Li, S. Chen, H. Yan, C. Wang, C. Wu, Y. A. Haleem, S. Duan, J. Lu and B. Ge, Atomically dispersed platinum supported on curved carbon supports for efficient electrocatalytic hydrogen evolution, *Nat. Energy*, 2019, **4**(6), 512.
12 N. Cheng, S. Stambula, D. Wang, M. N. Banis, J. Liu, A. Riese, B. Xiao, R. Li, T.-K. Sham and L.-M. Liu, Platinum single-atom and cluster catalysis of the hydrogen evolution reaction, *Nat. Commun.*, 2016, **7**(1), 1.
13 J. N. Tiwari, S. Sultan, C. W. Myung, T. Yoon, N. Li, M. Ha, A. M. Harzandi, H. J. Park, D. Y. Kim and S. S. Chandrasekaran, Multicomponent electrocatalyst with ultralow Pt loading and high hydrogen evolution activity, *Nat. Energy*, 2018, **3**(9), 773.
14 X. P. Yin, H. J. Wang, S. F. Tang, X. L. Lu, M. Shu, R. Si and T. B. Lu, Engineering the coordination environment of single-atom platinum anchored on graphdiyne for optimizing electrocatalytic hydrogen evolution, *Angew. Chem., Int. Ed.*, 2018, **57**(30), 9382.
15 N. Xuan, J. Chen, J. Shi, Y. Yue, P. Zhuang, K. Ba, Y. Sun, J. Shen, Y. Liu and B. Ge, Single-Atom Electroplating on Two Dimensional Materials, *Chem. Mater.*, 2018, **31**(2), 429.
16 J. Deng, H. Li, J. Xiao, Y. Tu, D. Deng, H. Yang, H. Tian, J. Li, P. Ren and X. Bao, Triggering the electrocatalytic hydrogen evolution activity of the inert two-dimensional MoS 2 surface *via* single-atom metal doping, *Energy Environ. Sci.*, 2015, **8**(5), 1594.
17 H. Wei, X. Liu, A. Wang, L. Zhang, B. Qiao, X. Yang, Y. Huang, S. Miao, J. Liu and T. Zhang, FeO x-supported platinum single-atom and pseudo-single-atom catalysts for chemoselective hydrogenation of functionalized nitroarenes, *Nat. Commun.*, 2014, **5**, 5634.
18 H. Wang, J.-X. Liu, L. F. Allard, S. Lee, J. Liu, H. Li, J. Wang, J. Wang, S. H. Oh and W. Li, Surpassing the single-atom catalytic activity limit through paired Pt-O-Pt ensemble built from isolated Pt 1 atoms, *Nat. Commun.*, 2019, **10**(1), 1.
19 S. Fang, X. Zhu, X. Liu, J. Gu, W. Liu, D. Wang, W. Zhang, Y. Lin, J. Lu and S. Wei, Uncovering near-free platinum single-atom dynamics during electrochemical hydrogen evolution reaction, *Nat. Commun.*, 2020, **11**(1), 1.
20 H. Luo, Y. Liu, S. D. Dimitrov, L. Steier, S. Guo, X. Li, J. Feng, F. Xie, Y. Fang and A. Sapelkin, Pt single-atoms supported on nitrogen-doped carbon dots for highly efficient photocatalytic hydrogen generation, *J. Mater. Chem. A*, 2020, **8**(29), 14690.
21 H. Liu, X. Peng and X. Liu, Single-Atom Catalysts for the Hydrogen Evolution Reaction, *ChemElectroChem*, 2018, **5**(20), 2963.
22 J. Ji, Y. Zhang, L. Tang, C. Liu, X. Gao, M. Sun, J. Zheng, M. Ling, C. Liang and Z. Lin, Platinum single-atom and cluster anchored on functionalized MWCNTs with ultrahigh mass efficiency for electrocatalytic hydrogen evolution, *Nano Energy*, 2019, **63**, 103849.
23 Z.-Y. Zhou, N. Tian, Z.-Z. Huang, D.-J. Chen and S.-G. Sun, Nanoparticle catalysts with high energy surfaces and enhanced activity synthesized by electrochemical method, *Faraday Discuss.*, 2009, **140**, 81.
24 C. Xiao, B.-A. Lu, P. Xue, N. Tian, Z.-Y. Zhou, X. Lin, W.-F. Lin and S.-G. Sun, High-index-facet-and high-surface-energy nanocrystals of metals and metal oxides as highly efficient catalysts, *Joule*, 2020, 2562–2598.
25 Z.-Y. Yu, R. Huang, J. Liu, C.-X. Luo, C.-Y. Wang, Q.-T. Song, C. Xiao, S.-H. Yin, B.-B. Xu and S.-G. Sun, PdPt concave nanocubes directly electrodeposited on carbon paper as high active and durable catalysts for formic acid and ethanol oxidation, *Electrochim. Acta*, 2020, **354**, 136654.
26 N. Tian, Z.-Y. Zhou and S.-G. Sun, Electrochemical preparation of Pd nanorods with high-index facets, *Chem. Commun.*, 2009, (12), 1502.
27 N. Tian, Z.-Y. Zhou and S.-G. Sun, Platinum metal catalysts of high-index surfaces: from single-crystal planes to electrochemically shape-controlled nanoparticles, *J. Phys. Chem. C*, 2008, **112**(50), 19801.
28 N. Tian, Z.-Y. Zhou, S.-G. Sun, Y. Ding and Z. L. Wang, Synthesis of tetrahexahedral platinum nanocrystals with high-index facets and high electro-oxidation activity, *science*, 2007, **316**(5825), 732.
29 Y. Zhang, F. Gao, P. Song, J. Wang, J. Guo, Y. Shiraishi and Y. Du, Glycine-assisted fabrication of N-doped graphene-supported uniform multipetal PtAg nanoflowers for enhanced ethanol and ethylene glycol oxidation, *ACS Sustainable Chem. Eng.*, 2019, **7**(3), 3176.

30 Y. Uemura, Y. Inada, K. K. Bando, T. Sasaki, N. Kamiuchi, K. Eguchi, A. Yagishita, M. Nomura, M. Tada and Y. Iwasawa, Core–Shell Phase Separation and Structural Transformation of Pt3Sn Alloy Nanoparticles Supported on γ-Al2O3 in the Reduction and Oxidation Processes Characterized by *In Situ* Time-Resolved XAFS, *J. Phys. Chem. C*, 2011, **115**(13), 5823.

31 N. Ishiguro, T. Saida, T. Uruga, S.-i. Nagamatsu, O. Sekizawa, K. Nitta, T. Yamamoto, S.-i. Ohkoshi, Y. Iwasawa and T. Yokoyama, Operando time-resolved X-ray absorption fine structure study for surface events on a Pt3Co/C cathode catalyst in a polymer electrolyte fuel cell during voltage-operating processes, *ACS Catal.*, 2012, **2**(7), 1319.

32 J. Ohyama, K. Teramura, Y. Higuchi, T. Shishido, Y. Hitomi, K. Kato, H. Tanida, T. Uruga and T. Tanaka, In situ observation of nucleation and growth process of gold nanoparticles by quick XAFS spectroscopy, *ChemPhysChem*, 2011, **12**(1), 127.

33 M. Wang, L. Árnadóttir, Z. J. Xu and Z. Feng, In situ X-ray absorption spectroscopy studies of nanoscale electrocatalysts, *Nano-Micro Lett.*, 2019, **11**(1), 47.

34 T. Lin, T. Huang, Y. Liu, C. Yeh, Y. Lai and W.-H. Hung, Adsorption and reaction of methanethiol on Pt (1 1 1), *Surf. Sci.*, 2005, **578**(1–3), 27.

35 K. Asakura, T. Kubota, W.-J. Chun, Y. Iwasawa, K. Ohtani and T. Fujikawa, Pt L3-edge XANES studies about the hydrogen adsorption on small Pt particles, *J. Synchrotron Radiat.*, 1999, **6**(3), 439.

36 L. Zhang, A. Wang, J. T. Miller, X. Liu, X. Yang, W. Wang, L. Li, Y. Huang, C.-Y. Mou and T. Zhang, Efficient and durable Au alloyed Pd single-atom catalyst for the Ullmann reaction of aryl chlorides in water, *ACS Catal.*, 2014, **4**(5), 1546.

37 M. P. Seah and W. Dench, Quantitative electron spectroscopy of surfaces: A standard data base for electron inelastic mean free paths in solids, *Surf. Interface Anal.*, 1979, **1**(1), 2.

38 C. Kuppe, K. R. Rusimova, L. Ohnoutek, D. Slavov and V. K. Valev, "Hot" in Plasmonics: Temperature-Related Concepts and Applications of Metal Nanostructures, *Adv. Opt. Mater.*, 2020, **8**(1), 1901166.

39 P. N. Duchesne, Z. Li, C. P. Deming, V. Fung, X. Zhao, J. Yuan, T. Regier, A. Aldalbahi, Z. Almarhoon and S. Chen, Golden single-atomic-site platinum electrocatalysts, *Nat. Mater.*, 2018, **17**(11), 1033.

40 P. Swetha and S.-P. Feng, High-index facet defined shape-controlled electrochemical synthesis of nanocrystals: A mini review, *Electrochem. Commun.*, 2018, **94**, 64.

41 Y. Zheng, Y. Jiao, Y. Zhu, L. H. Li, Y. Han, Y. Chen, M. Jaroniec and S.-Z. Qiao, High electrocatalytic hydrogen evolution activity of an anomalous ruthenium catalyst, *J. Am. Chem. Soc.*, 2016, **138**(49), 16174.

42 L. Zhang, Y. Jia, G. Gao, X. Yan, N. Chen, J. Chen, M. T. Soo, B. Wood, D. Yang and A. Du, Graphene defects trap atomic Ni species for hydrogen and oxygen evolution reactions, *Chem*, 2018, **4**(2), 285.

43 X. Yan, H. Li, J. Sun, P. Liu, H. Zhang, B. Xu and J. Guo, Pt nanoparticles decorated high-defective graphene nanospheres as highly efficient catalysts for the hydrogen evolution reaction, *Carbon*, 2018, **137**, 405.

44 F.-H. Cho, Y.-C. Lin and Y.-H. Lai, Electrochemically fabricated gold dendrites with high-index facets for use as surface-enhanced Raman-scattering-active substrates, *Appl. Surf. Sci.*, 2017, **402**, 147.

45 U.-S. Jeng, C. H. Su, C.-J. Su, K.-F. Liao, W.-T. Chuang, Y.-H. Lai, J.-W. Chang, Y.-J. Chen, Y.-S. Huang and M.-T. Lee, A small/wide-angle X-ray scattering instrument for structural characterization of air–liquid interfaces, thin films and bulk specimens, *J. Appl. Crystallogr.*, 2010, **43**(1), 110.

